Biochimica et Biophysica Acta 1807 (2011) 1606–1615

Contents lists available at SciVerse ScienceDirect

Biochimica et Biophysica Acta

journal homepage: www.elsevier.com/locate/bbabio

X-ray structure of the dimeric cytochrome bc_1 complex from the soil bacterium *Paracoccus denitrificans* at 2.7-Å resolution

Thomas Kleinschroth [a,b,*], Michela Castellani [b], Chi H. Trinh [c], Nina Morgner [d], Bernhard Brutschy [d], Bernd Ludwig [b], Carola Hunte [a,*]

[a] Institute for Biochemistry and Molecular Biology, ZMBZ, BIOSS Centre for Biological Signalling Studies, Stefan-Meier-Strasse 17, Albert-Ludwigs-University, 79104 Freiburg, Germany
[b] Institute of Biochemistry, Molecular Genetics, Goethe University, 60438 Frankfurt am Main and Cluster of Excellence Macromolecular Complexes Frankfurt am Main (CEF), Max-von-Laue-Strasse 9, 60438 Frankfurt am Main, Germany
[c] Astbury Centre for Structural Molecular Biology, University of Leeds, LS2 9JT Leeds, UK
[d] Department of Physical and Theoretical Chemistry, Goethe University, 60438 Frankfurt am Main and Cluster of Excellence Macromolecular Complexes Frankfurt am Main (CEF), Max-von-Laue-Strasse 7, 60438 Frankfurt am Main, Germany

ARTICLE INFO

Article history:
Received 17 June 2011
Received in revised form 21 September 2011
Accepted 27 September 2011
Available online 3 October 2011

Keywords:
Respiratory complex III
Rhodobacteraceae
Stigmatellin
LILBID
Membrane protein structure

ABSTRACT

The respiratory cytochrome bc_1 complex is a fundamental enzyme in biological energy conversion. It couples electron transfer from ubiquinol to cytochrome *c* with generation of proton motive force which fuels ATP synthesis. The complex from the α-proteobacterium *Paracoccus denitrificans*, a model for the medically relevant mitochondrial complexes, lacked structural characterization. We show by LILBID mass spectrometry that truncation of the organism-specific, acidic N-terminus of cytochrome c_1 changes the oligomerization state of the enzyme to a dimer. The fully functional complex was crystallized and the X-ray structure determined at 2.7-Å resolution. It has high structural homology to mitochondrial complexes and to the *Rhodobacter sphaeroides* complex especially for subunits cytochrome *b* and ISP. Species-specific binding of the inhibitor stigmatellin is noteworthy. Interestingly, cytochrome c_1 shows structural differences to the mitochondrial and even between the two *Rhodobacteraceae* complexes. The structural diversity in the cytochrome c_1 surface facing the ISP domain indicates low structural constraints on that surface for formation of a productive electron transfer complex. A similar position of the acidic N-terminal domains of cytochrome c_1 and yeast subunit QCR6p is suggested in support of a similar function. A model of the electron transfer complex with membrane-anchored cytochrome c_{552}, the natural substrate, shows that it can adopt the same orientation as the soluble substrate in the yeast complex. The full structural integrity of the *P. denitrificans* variant underpins previous mechanistic studies on intermonomer electron transfer and paves the way for using this model system to address open questions of structure/function relationships and inhibitor binding.

1. Introduction

The enzyme ubihydroquinone: cytochrome *c* oxidoreductase (E.C.1.10.2.2) or cytochrome bc_1 complex (cyt bc_1 complex) is a central component of the energy conversion machinery of respiratory and photosynthetic electron transfer chains. The multi-subunit membrane protein complex couples electron transfer from hydroquinone to cytochrome *c* (cyt *c*) to the translocation of protons across the membrane in a mechanism called Q cycle, thereby substantially contributing to the proton motive force that is used for ATP synthesis [1]. The complex is a target for numerous inhibitors including antimalarial drugs [2,3] and agrochemical fungicides [4] and is implicated in the biological processes of aging mediated by reactive oxygen species (ROS) [5]. X-ray structures of mitochondrial complexes from vertebrates [6–8] and yeast [9,10] and of bacterial complexes from *Rhodobacter sphaeroides* [11] and *R. capsulatus* [12] provided critical information for elucidation of mechanism and structure/function relationships. Yet, the *R. sphaeroides* complex lacks its supernumerary subunit IV in the structure. Loss of this subunit lowers the enzyme activity of detergent-solubilized complex to 26% as compared to the wild-type complex [11,13]. The structure of *R. capsulatus* is complete with its three subunits but lacks amino acid residue side chains due to the limited resolution of 3.8 Å [12]. Important details of the cyt bc_1 complex mechanism and its regulation are still not fully understood, especially those of ubiquinol oxidation, equilibration of electrons between functional units and related bypass reactions that generate ROS. The minimal functional unit of the enzyme is theoretically a monomer comprising the three redox-active subunits cytochrome *b* (cyt *b*), cytochrome c_1 (cyt c_1) and the Rieske iron sulphur protein

Abbreviations: [2Fe–2S] cluster, two iron two sulphur cluster; ac, acidic domain; cyt, cytochrome; ET, electron transfer; ISP, iron sulphur protein; ROS, reactive oxygen species; SU, subunit; TMH, transmembrane helix

* Corresponding authors at: Institute for Biochemistry and Molecular Biology, ZMBZ, BIOSS Centre for Biological Signalling Studies, Stefan-Meier-Strasse 17, Albert-Ludwigs-University, 79104 Freiburg, Germany. Tel.: +49 761 2035279.
E-mail addresses: thomas.kleinschroth@biochemie.uni-freiburg.de (T. Kleinschroth), carola.hunte@biochemie.uni-freiburg.de (C. Hunte).

0005-2728/$ – see front matter © 2011 Elsevier B.V. All rights reserved.
doi:10.1016/j.bbabio.2011.09.017

(ISP) with their respective cofactors heme b_H, heme b_L, heme c_1 and the [2Fe–2S] cluster. The ISP connects two functional units to an obligate dimer, as its transmembrane helix (TMH) is anchored to one monomer and the catalytic head domain interacts with the other. In addition, the movement of the ISP head domain is essential for the mechanism. The [2Fe–S] cluster receives an electron when the head domain docks onto cyt *b* in the so-called *b*-position, and it is reoxidized by cyt c_1 after the domain reorients towards the latter into its *c*-position.

The cyt bc_1 complex of the soil bacterium *Paracoccus denitrificans* is elementary in its subunit composition comprising the three redox-active subunits which are encoded by the *fbc*-operon [14]. The electron acceptor in this gram-negative α-proteobacterium is the membrane-anchored cytochrome c_{552}. The *P. denitrificans* complex is biochemically and kinetically well characterized [15–18] and genetically readily accessible in contrast to the larger mitochondrial complexes with several supernumerary subunits, for which especially mutagenesis of mitochondrially encoded cyt *b* is laborious. The complex provides an ideal model system. Interestingly, subunit cyt c_1 has an organism-specific N-terminal domain with a very unusual amino acid composition of 40% alanine, 14% proline and 38% negatively charged amino acid residues [14]. This results most likely in a flexible domain without predicted secondary structural elements and high negative charge at physiological pH value. This domain of amino acid residues 39–203 was genetically deleted from the *fbc*C gene. The resulting cyt $bc_1^{\Delta ac}$ complex is fully active and was successfully used in a mechanistic study [19] that provided strong evidence for electron transfer between the two monomers, thus supporting the half-of-the-sites-mechanism in which one monomer is active at a time, a potential regulatory process [20]. In native and in partially solubilized membranes, the wild-type complex is present in supramolecular association known as supercomplex or respirasome with a stoichiometry of 1:4:4 for complexes I, III and IV of the respiratory chain, respectively [21]. Furthermore, the wild-type cyt bc_1 complex has the mass of a tetramer in detergent-solubilized form, a state described as dimer-of-dimers [22].

In this study, the cyt $bc_1^{\Delta ac}$ complex was produced, purified and analysed to be an intact dimer. The complex was crystallized in the presence of the inhibitor stigmatellin and the X-ray structure of the enzyme was determined. The structure allowed not only comparison with highly homologous mitochondrial complexes but also between two enzymes of the same bacterial family, the *Rhodobacteraceae*, revealing that subunit cyt c_1 is structurally more diverse than the other catalytic subunits of the complexes [23,24].

A model of the cyt bc_1 complex in interaction with cyt c_{552} provides insight in the architecture of the natural electron transfer complex and its integration in respiratory supercomplexes.

2. Materials and methods

2.1. Cloning, production and purification

Recombinant cyt $bc_1^{\Delta ac}$ complex [25] of *P. denitrificans* fused with a C-terminal deca-histidine-tag at cyt *b* was produced by homologous expression and purified by single-step immobilized-metal-affinity chromatography. Details of cloning, production and purification were described previously [19]. The concentrated complex was applied to a size-exclusion chromatography (SEC) column (TSK4000SW, Tosoh) equilibrated with 25 mM NaPi pH 7.5, 250 mM NaCl and 0.02% β-D-dodecyl-malto-pyranoside (DDM) and eluted with the same buffer. The central fractions of the elution peak were pooled. Stigmatellin was added in 10-fold molar excess and the complex concentrated to 40 mg/mL.

2.2. LILBID analysis

The laser-induced liquid-bead ion-desorption (LILBID) mass spectrometry permits analysis of the weight of intact macromolecular detergent-solubilized transmembrane complexes and of their individual subunits as described previously [22], and more recently has been used to determine the size of several other membrane proteins [26,27]. The bc_1 complex was solubilized with DDM and purified as described above with the exception that stigmatellin addition was omitted. For the analysis, the buffer was exchanged by size exclusion chromatography for ammonium acetate buffer with 0.02% of DDM and the complex concentrated to 2 μM. Droplets of this solution were introduced into vacuum and then radiated with a laser beam with the wavelength of 3 μm. The desorption-energy can be varied between 1 and 15 mJ/pulse permitting to adjust different soft or harsh conditions. We recorded spectra under low and mid-high laser intensity. For detecting the large biomolecules, the LILBID instrument is equipped with a Daly-type ion detector with a resolution range in the low mega Dalton range. The final spectra are typically averages of 100–200 shots or droplets, respectively. Here, we recorded spectra under low and mid-high laser intensity.

2.3. 3D-structure

2.3.1. Crystallization

For crystallization, the cyt bc_1 complex was diluted to 20 mg/mL with the same buffer adding sucrose to a final concentration of 1 M. The sample was ultra-centrifuged at 110,000 *g* for 30 min to remove initial precipitate, and was crystallized in a hanging-drop vapour diffusion set-up in 24 well-plates. 100 mM sodium acetate, pH 4.6, 50 mM NaCl, 30% (+/−)-2-methyl-2,4-pentandiol (MPD) was used as reservoir solution. The protein sample was mixed 1:2 with reservoir solution containing 33% MPD. Typically, red crystals formed within 4 days of incubation at 18 °C. Crystals were harvested with cryo-loops and immediately flash-cooled and stored in liquid nitrogen.

2.3.2. Data collection and processing

Data were recorded to a resolution of 2.7 Å from a single crystal at 100 K on the macromolecular crystallography beamline station I03 at Diamond Light Source. The diffraction images were integrated using MOSFLM [28] and scaled and truncated using SCALA [29] and CTRUNCATE [30], respectively. Five percent of the reflections were randomly selected and excluded from the refinement using the program FREERFLAG [31] and constituted the R_{free} set. The data processing statistics are shown in Table 1.

2.3.3. Structure determination

The crystal structure was determined by molecular replacement using the program PHASER [32] with the structure of the cyt bc_1 complex from the photosynthetic bacterium *R. sphaeroides* as the search model (PDB ID 2QJY [11]). After initial rounds of rigid body and restrained refinements using REFMAC5, [33] the polypeptide chain was modified to the *P. denitrificans* residues and checked against both $2F_o–F_c$ and $F_o–F_c$ electron density maps in the program COOT [34]. Residues of regions that are structurally different between the *P. denitrificans* and *R. sphaeroides* sequences were removed to prevent bias in map generation. Iterative manual model building and refinement were carried out using COOT and REFMAC5 permitting some of the deleted regions to be rebuilt. Numbering of cyt $c_1^{\Delta ac}$ residues is based on the sequence of the variant (Fig. S1).

The initial coordinates for the cofactors were obtained from the *R. sphaeroides* cyt bc_1 complex structure (PDB ID 2QJY) and the restraint library file for the inhibitor stigmatellin was obtained from the PRODRG server [35]. All ligands were manually fitted into both $2F_o–F_c$ and $F_o–F_c$ maps in the program COOT. Water molecules were manually added in COOT for peaks over 3.0 σ in the $F_o–F_c$ map and the structure validation carried out with MOLPROBITY [36]. The refinement statistics are shown in Table 1. All figures with presentations of structures have been made with VMD [37] containing

Table 1
Data collection, processing and refinement statistics.

Data collection	
Synchrotron	Diamond Light Source
Beamline	I03
Wavelength (Å)	0.97
Resolution range (Å)[a]	98.0–2.70 (2.85–2.70)
Space group	$P2_1$
Unit cell	
a, b, c (Å)	85.3, 164.9, 100.6
α, β, γ (°)	90.0, 103.2, 90.0
No. of observed reflections	218,227
No. of unique reflections	70,055
Redundancy	3.1 (3.1)
Completeness (%) [a]	94.6 (90.0)
$< I/\sigma(I) >$[a]	5.7 (2.9)
R_{merge} (%)[b a]	12.9 (32.2)
Refinement	
Resolution range for refinement (Å)	98.0–2.70
R factor (%)	23.8
R_{free} (%)[c]	29.1
No. of protein non-H atoms	12,644
No. of water molecules	6
No. of non-protein non-H atoms	340
RMSD bond lengths (Å)[d]	0.015
RMSD bond angles (°)[d]	1.8
Average overall *B* factor (Å^2)	
Protein	29
Water	15
Non-protein	20
Ramachandran analysis (%) [e]	
Most favoured	92.1
Outliers	1.4
PDB ID	2YIU

[a] Values given in parentheses correspond to those in the outermost shell of the resolution range.
[b] $R_{merge} = \sum_{hkl}\sum_i |I_i(hkl) - \langle I(hkl)\rangle| / \sum_{hkl}\sum I_i(hkl)$.
[c] R_{free} was calculated with 5% of the reflections set aside randomly.
[d] Based on the ideal geometry values of Engh and Huber [60].
[e] Ramachandran analysis using the program MOLPROBITY [36].

the secondary structure package [38] or Pymol. Root mean square deviations given refer to deviations on C_α-atoms.

2.3.4. Accession numbers

Coordinates and structure factors have been deposited in the PDB with accession code PDB ID: 2YIU.

3. Results and discussion

3.1. The dimeric cyt bc_1 complex

The cyt bc_1 complex of the mesophilic soil bacterium *P. denitrificans* is a widely accepted prokaryotic model for the mitochondrial respiratory complex [15–17,19]. The recombinant complex is biochemically and functionally well characterized [19]. The His-tagged variant can be readily prepared at high purity and has wild-type properties [16]. Both, wild-type and His-tagged complex have resisted crystallization in more than 25,000 trials screening a broad range of conditions. Yet, a variant of the complex, cyt $bc_1^{\Delta ac}$ [19], which lacks the organism-specific N-terminal domain of cyt c_1 (amino acid residues 39 to 203) but retains the N-terminus including the predicted cyt c_1 signal sequence (residues 1–24 [14]), was successfully crystallized. The cyt $bc_1^{\Delta ac}$ complex is fully functional with very similar kinetic features as compared to the wild type complex judged by V_{max}, k_{cat} and presteady-state kinetics [19].

Interestingly, the major difference between wild type and cyt $bc_1^{\Delta ac}$ complex is the oligomerization state of the detergent solubilized form, which can explain the difference in crystallization properties. The wild type complex is a dimer-of-dimers as determined by laser-induced liquid-bead ion-desorption (LILBID)-mass spectrometry [22]. In contrast, SEC and blue native-PAGE analysis (data not shown) indicate that the cyt $bc_1^{\Delta ac}$ complex is a dimer. This was verified by LILBID mass spectrometry (Fig. 1A). The spectrum at low laser intensity clearly shows a characteristic peak series of an intact dimeric complex starting with a single charged peak at 200 kDa corresponding well to the calculated dimer mass of 205 kDa. At higher laser intensity, individual subunits and subcomplexes are resolved with their correct masses (Fig. 1B) including that of the truncated subunit cyt $c_1^{\Delta ac}$ (Rieske protein, cyt *b*, cyt $c_1^{\Delta ac}$ with LILBID/theoretical masses of 20.1/20.4, 50.8/53.0 and 28.7/29.1 kDa, respectively). The functional unit of the cyt bc_1 complex is the dimer, as catalytic domain and transmembrane anchor of the Rieske protein are associated with the respective opposite monomer (Fig. 2) [39]. Though the dimer-of-dimers complex is active, it is not known how the most likely largely disordered acidic domain mediates the larger association and which function the oligomerization may have. In the membrane, the *P. denitrificans* cyt bc_1 complex is associated in respiratory supercomplexes [21] which are also known for the mitochondrial complexes [40]. A stoichiometry of 1:4:4 was determined for the *P. denitrificans* supercomplex I/III/IV [21] suggesting that this cyt bc_1 complex is also a dimer-of-dimers in the membrane.

3.2. Crystallization and crystal lattice

Single crystals of the cyt $bc_1^{\Delta ac}$ complex were grown in vapour-diffusion set-ups. Growth in the presence of the cryo-protectant

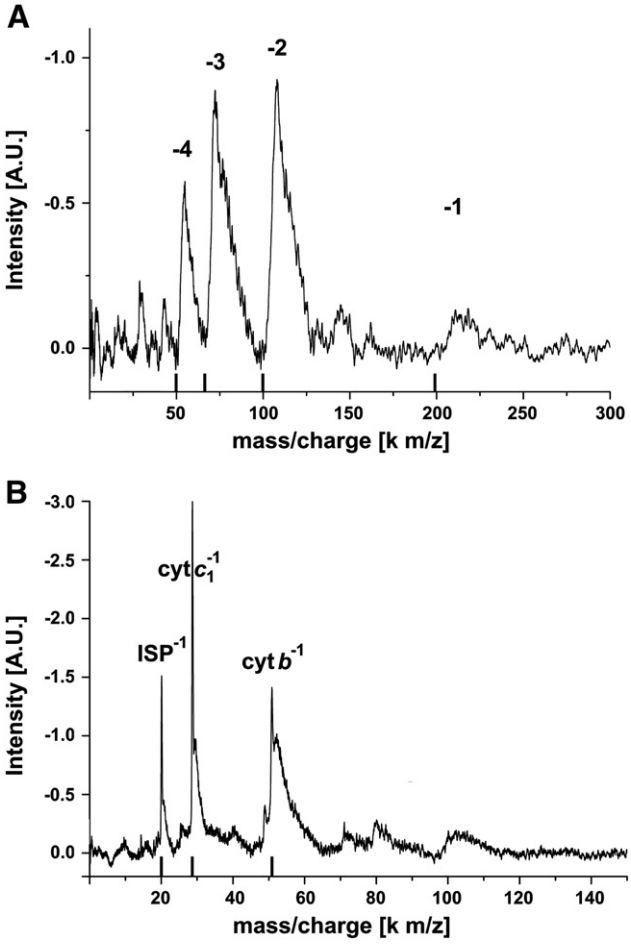

Fig. 1. LILBID-mass spectra of the cyt $bc_1^{\Delta ac}$ complex. (A) The complex remains intact at soft desorption conditions with a characteristic mass-over-charge peak series due to the charge distribution from right to left. It starts with the lowest peak of the single charged complex at 200 kDa. (B) At harsh desorption conditions, the three subunits of the complex are resolved as singly charged species close to their theoretical masses. Subunit cyt $c_1^{\Delta ac}$ is correctly resolved at its calculated mass (29 kDa). Smaller peaks in the higher mass range are contributed by subcomplexes.

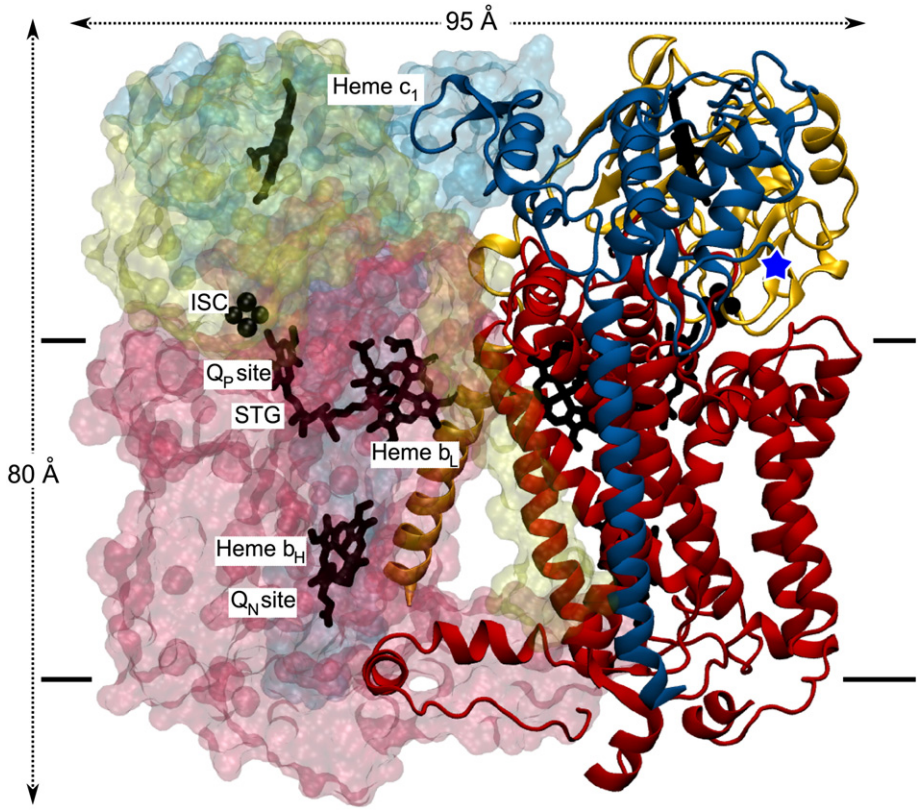

Fig. 2. X-ray structure at 2.7 Å resolution of the dimeric *P. denitrificans* cyt $bc_1^{\Delta ac}$ complex. The left monomer of the complex is shown in a transparent surface representation. The right monomer is depicted as C_α trace with secondary structure elements. Cofactors and the inhibitor stigmatellin (STG) are shown in stick-and-ball representation. The colour code is cyt *b* in red, cyt c_1 in blue and ISP in yellow. The cofactors and the bound stigmatellin are shown in black. The position of the membrane is indicated with black horizontal lines. The molecule is viewed parallel to the membrane with the cytoplasmic side at the bottom. Labelling for cofactors, inhibitor and Q sites are given for one monomer only. The resolved N-terminus of cyt $c_1^{\Delta ac}$ is marked with a blue asterisk.

sucrose was essential to minimize handling of the crystals during harvest and cryo-cooling as to maintain diffraction properties of the very fragile crystals. Diffraction data were recorded, phases were obtained by molecular replacement and the structure was refined at a resolution of 2.7 Å (Table 1). The cyt $bc_1^{\Delta ac}$ complex is present as dimer in the asymmetric unit (Fig. 3) in line with the oligomerization state identified by LILBID mass spectrometry. The molecules form ordered stacks of two-dimensional (2D) crystalline layers, so called type-I crystals [41]. The latter are commonly observed for membrane proteins crystallized in lipid mesophases [42], but are unusual for

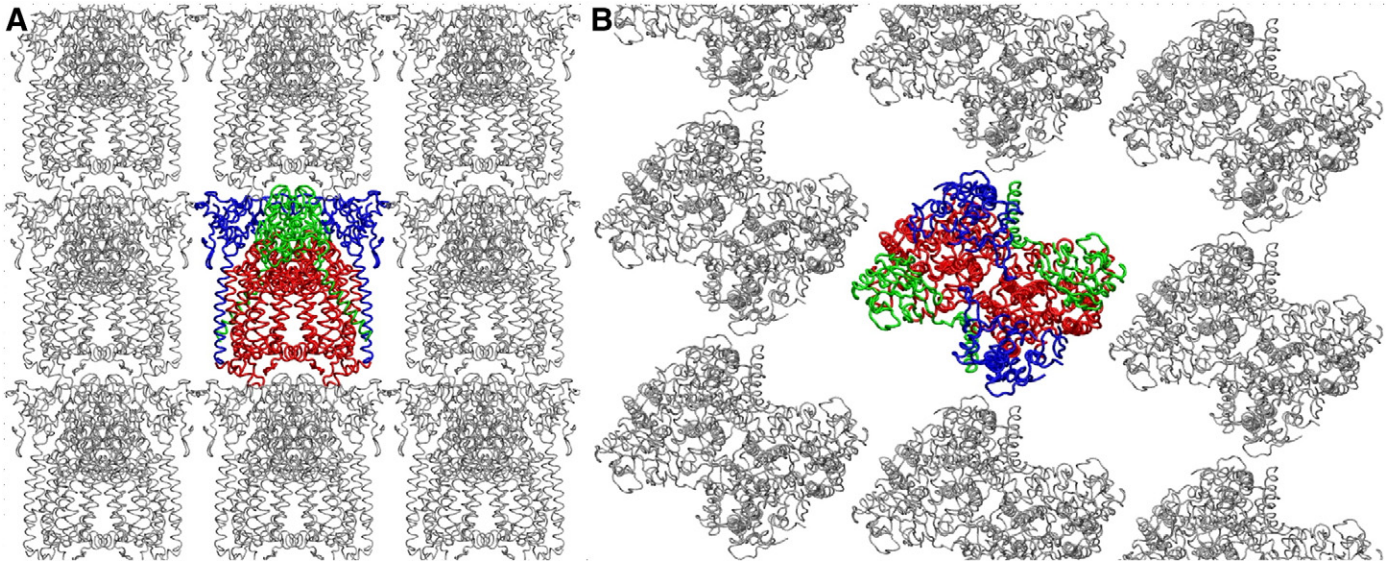

Fig. 3. Crystal lattice of the cyt $bc_1^{\Delta ac}$ complex. The central molecule and one layer of neighbouring molecules are shown in the following colours: cyt *b* in red, cyt c_1 in blue and ISP in green. The symmetry molecules are shown in gray. A) crystal lattice (a, b plane) viewed in c direction. The two-dimensional, ordered layers of cyt bc_1 complexes are tightly stacked with multiple non-polar interactions of atoms between the layers. B) Crystal lattice (a, c plane) viewed in b direction. Large solvent space is present between the complexes, with two weak interactions stabilizing the packing.

proteins in detergent as the transmembrane domain is covered by a detergent micelle preventing crystal contacts in the hydrophobic region. The stacks of 2D-layers of cyt $bc_1^{\Delta ac}$ molecules are tightly packed with multiple non polar interactions of atoms in van-der-Waals contact distance between the layers (Fig. 3A). Residues of the N-terminus of cyt *b* are in contact to ISP (Gly3$^{cyt\ b}$:Asp183^{ISP}, Pro5$^{cyt\ b}$:Leu182^{ISP}) and to cyt c_1 (Gly3$^{cyt\ b}$:Glu141$^{cyt\ c1\Delta ac}$). Residues of the *de* loop of cyt *b* interact with the extrinsic ISP domain (Gly232$^{cyt\ b}$:Glu83^{ISP}, Gly232$^{cyt\ b}$:Asp84^{ISP}). Contacts are present between the different cytochromes (Met422$^{cyt\ b}$:Ala111$^{cyt\ c1\Delta ac}$) and helix H of cyt *b* and the extrinsic domain of ISP (Ala419$^{cyt\ b}$:Glu62^{ISP}). In contrast, few interactions between neighbouring molecules are present within the 2D-layer (Fig. 3B). A weak interaction is present between the *ef* loop of cyt *b* and the helix H of the neighbouring cyt *b* (Tyr391$^{cyt\ b}$:Trp313$^{cyt\ b}$) on the periplasmic side of the protein. A second interaction is present between the same residues of two adjacent cyt c_1 molecules (Asp223$^{cyt\ c1\Delta ac}$). The molecules within the 2D-layer are tightly packed in one orientation with about ~11-Å closest distance in the transmembrane region implying that the detergent micelles are locally displaced. They are very loosely packed with large cavities in the orthogonal direction resulting in a high solvent content (57.8%). The loose packing may explain the fragile nature of the crystals.

3.3. Structure determination and overall structure

The structure of *P. denitrificans* cyt $bc_1^{\Delta ac}$ was determined at 2.7-Å resolution. Phases were obtained by molecular replacement with the homologous bacterial cyt bc_1 complex from *R. sphaeroides*, which is also a member of the *Rhodobacteraceae* family. The final structure of the *P. denitrificans* complex is very well defined and comprises subunits cyt *b*, cyt $c_1^{\Delta ac}$ and ISP and their respective cofactors heme b_L, heme b_H, heme c_1, [2Fe–2S]-cluster and the Q_P site inhibitor stigmatellin (Fig. 2). The overall fold is highly similar to the catalytic subunits of the mitochondrial complexes as demonstrated by superimposition with the corresponding subunits of the yeast cyt bc_1 complex (PDB ID 3CX5) [43]. Lowest deviations are observed for the highly conserved subunits cyt *b* and ISP with root mean square deviations of the C_α-atoms (RMSDs) of 0.8 Å and 1.1 Å, respectively. The sequence identity/similarity of cyt *b* and ISP is 49%/67% and 49%/62%, respectively, for comparison of these species (Figs. S2, S3). Cyt c_1 has a slightly higher RMSD of 1.3 Å in line with the lower sequence identity/similarity of 38%/47% based on the cyt $c_1^{\Delta ac}$ sequence (Fig. 4C). As expected, structural similarity is even more pronounced for the closely related *R. sphaeroides* complex with RMSDs of 0.37 Å, 0.58 Å, and 0.96 Å for cyt *b*, ISP and cyt c_1, respectively. This corresponds to higher sequence identities/similarities of 85%/92% (cyt *b*), 73%/86% (ISP) and 58%/67% (cyt $c_1^{\Delta ac}$, cyt c_1) for comparison of these species (Figs. 4C, S2, S3). Interestingly, cyt *b* and ISP of *P. denitrificans* are structurally more similar to the corresponding yeast subunits than the *R. sphaeroides* ones. RMSDs of 1.3 Å, 1.4 Å, and 1.3 Å were reported for cyt *b*, ISP, cyt c_1, respectively, when comparing the latter pair [11]. The slightly higher deviations of *P. denitrificans* cyt c_1 are in line with the notion, that subunits *b* and ISP form the evolutionary core of the *bc* complexes [23].

3.4. Cytochrome b

The two cyt *b* subunits form the hydrophobic core of the complex (Fig. 2). Each subunit is comprised of two bundles of 4 helixes, namely of TMH A–D and TMH E–H (TMH A: Trp43-His68, TMH B: Gly89-Tyr118, TMH C: Glu126-Trp51, TMH D: Asn188-Thr219, TMH E: Pro243-Phe269, TMH F: Ala328-Pro347, TMH G: Arg360-Met383, TMH H: Gly387-Ile414). Located within the first bundle are the two *b*-type hemes and their coordinating residues, His97 and His198 for heme b_L and His111 and His212 for heme b_H. The edge-to-edge distances between the cofactors relevant for electron transfer [44,45] are 11.9 Å between heme b_L and b_H within the monomer and 13.8 Å between b_L and b_L and 30.6 Å between b_H and b_H, respectively, within the dimer. Cyt *b* also holds the two reaction sites which are located on opposite sides of the membrane (Fig. 2). The Q_P site (ubiquinol oxidation) is facing the periplasmatic side and the Q_N site (ubiquinone reduction) is in the direction of the cytosolic side of the protein. The Q_P site can clearly be identified by the bound site-specific inhibitor stigmatellin. This reaction site is shielded against the aqueous phase as subunit ISP is docked onto cyt *b*. In agreement with the structure of the *R. sphaeroides* complex, cyt *b* has an extended N- and C-terminus and insertions in the loop regions DE and EF as compared to the mitochondrial complexes (Fig. S2). Both insertions contain a short helix (*ef*1 and *de* helix). Termini and DE insertion form a layer at the N-side of the membrane, which was discussed to stabilize the Q_N site environment and to prevent proton leakage in the bacterial complexes which lack supernumerary subunits on that side of the membrane [11].

3.5. The Rieske protein

Subunit ISP is made up of three domains. The membrane anchor is an N-terminal TMH (Asp17-Gln41) with pronounced tilt which brings the catalytic domain in contact with the second monomer providing the structural basis for the functional dimer (Fig. 2). The catalytic domain is interconnected with the TMH by the hinge region (Met42-Leu51), which harbours the ADV motif (Ala46-Val48, Fig. S3) that is conserved in ISP from *Saccharomyces cerevisiae*, *R. sphaeroides* and *P. denitrificans*. Mutations that affect length or rigidity of this part of the hinge region impair enzyme activity [46,47]. The C-terminal catalytic extrinsic domain consists of residues Ala52-Gly190. The fold of the domain is based on three β-sheets stacked as parallel layers. Sheet 2 and 3 hold the [2Fe–2S] cluster with the evolutionary conserved cluster coordinating residues His134, His155, Cys132 and Cys152. A clearly visible loop is formed by residues Ser101-Pro111. This insertion is typical for the prokaryotes from the *Rhodobacteraceae* family and is missing in the mitochondrial counterparts (Fig. S2).

3.6. Stigmatellin binding

The protein was crystallized in the presence of the competitive inhibitor stigmatellin. The orientation of the inhibitor was clearly visible in difference electron density maps prior to its inclusion in the model and permitted its unambiguous orientation and refinement. Stigmatellin binds in the distal position of the Q_P site between the cofactors heme b_L and the [2Fe–2S] cluster, in a pocket which is mainly formed by cyt *b* (Fig. 5A). It locks the mobile ISP head domain in the *b* position thus facilitating crystallization [9]. This is especially important as contacts between neighbouring molecules in the crystal lattice are mediated by ISP. The inhibitor is bound by two H-bonds and multiple interactions with atoms in van-der-Waals contact distance (Fig. 5B). Hydrogen bonds are present between the side chains of E295 of cyt *b* and His155 of ISP to the 8-hydroxy and the 4-oxo group of the chromone ring, respectively. Additional contacts to the chromone ring are contributed by cyt *b* (Met154, Gly158, Val161, Ile162, Ile292, Pro294, Phe298, Tyr302, and Met336) and by ISP (Cys154). The inhibitor is stably bound as indicated by an average B factor of 22.0 Å^2 as compared to 24.0 Å^2 for cyt *b*. Stabilization is most pronounced for the chromone ring (B factor 15.1 Å^2), with slightly increased B factor for the proximal tail (17.2 Å^2). The distal tail has least contacts and the highest B factor (33.9 Å^2). This partitioned stabilization is very similar to the one described for stigmatellin binding in the yeast cyt bc_1 complex [48]. Interestingly, binding interactions with stigmatellin in the *R. sphaeroides* complex appear to be more evenly distributed as indicated by similar B factors of the three moieties (55.1, 51.8, and 55.9 Å^2 for chromone ring, proximal and distal tail, respectively; as calculated from the structure of the *R. sphaeroides* complex, PDB 2QJP [11]). The inhibitor has a high affinity for all of the three species as suggested by IC_{50} determinations. An IC_{50} value of 130 nM was determined for

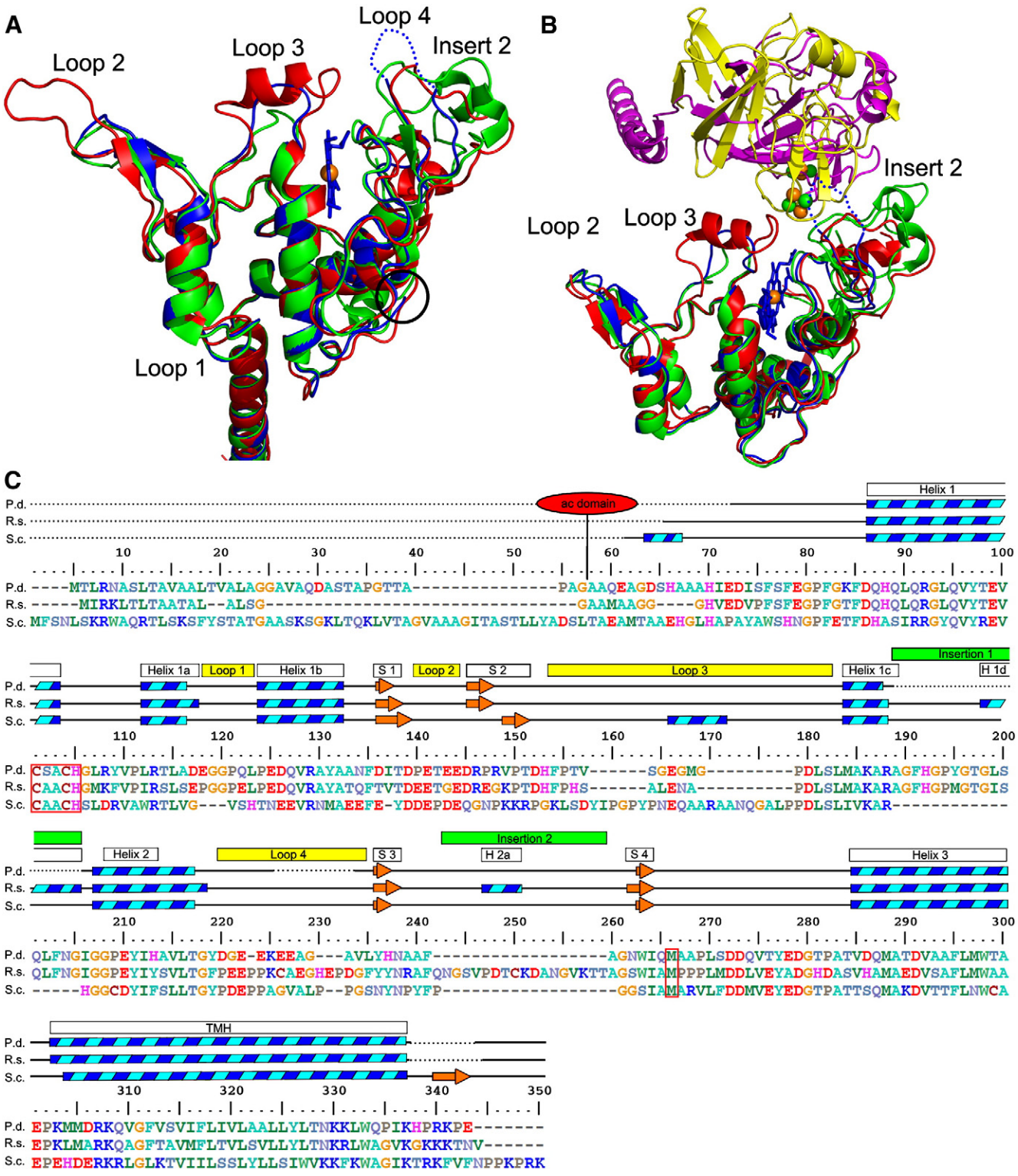

Fig. 4. Comparison of cyt $c_1^{\Delta ac}$ of *P. denitrificans* with cyt c_1 from *S. cerevisiae* and from *R. sphaeroides*. A) Superimposition of the Cα trace of the subunits from *P. denitrificans* (blue), *S. cerevisiae* (red), and *R. sphaeroides* (green) with the TMH pointing downwards. Differences are most pronounced in the labelled loop and insertion regions. The position of the flexible tip of loop 4 is shown in dotted line. The position of the resolved N-termini is indicated by the black circle. Heme c_1 is depicted for *P. denitrificans* only. B) Cyt c_1 — ISP interface. Superimposed cyt c_1 subunits as in A) are displayed with ISP of *P. denitrificans* in *b* position (magenta) and in modelled *c* position (yellow, superimposition on structure of bovine cyt bc_1 complex, PDB 1BE3 [50]). The ISP [2Fe–2S] cluster is shown as spheres. C) Sequence alignment of cyt $c_1^{\Delta ac}$ of *P. denitrificans* and cyt c_1 of *R. sphaeroides* and *S. cerevisiae* with secondary structural elements. Signal sequences are included. A comparison of the sequences of wild-type cyt c_1 with cyt $c_1^{\Delta ac}$ of *P. denitrificans* is shown in Fig. S1. Structural elements are indicated on top with cyan/blue striped boxes for α-helices and orange arrows for β-sheets. A dotted line indicates the absence of structural information. Insertions compared to the mitochondrial complex are shown as green boxes, characteristic loop regions are shown as yellow boxes. The red ellipse labelled *ac* domain indicates the position of the acidic domain present in *P. denitrificans* wild type cyt c_1.

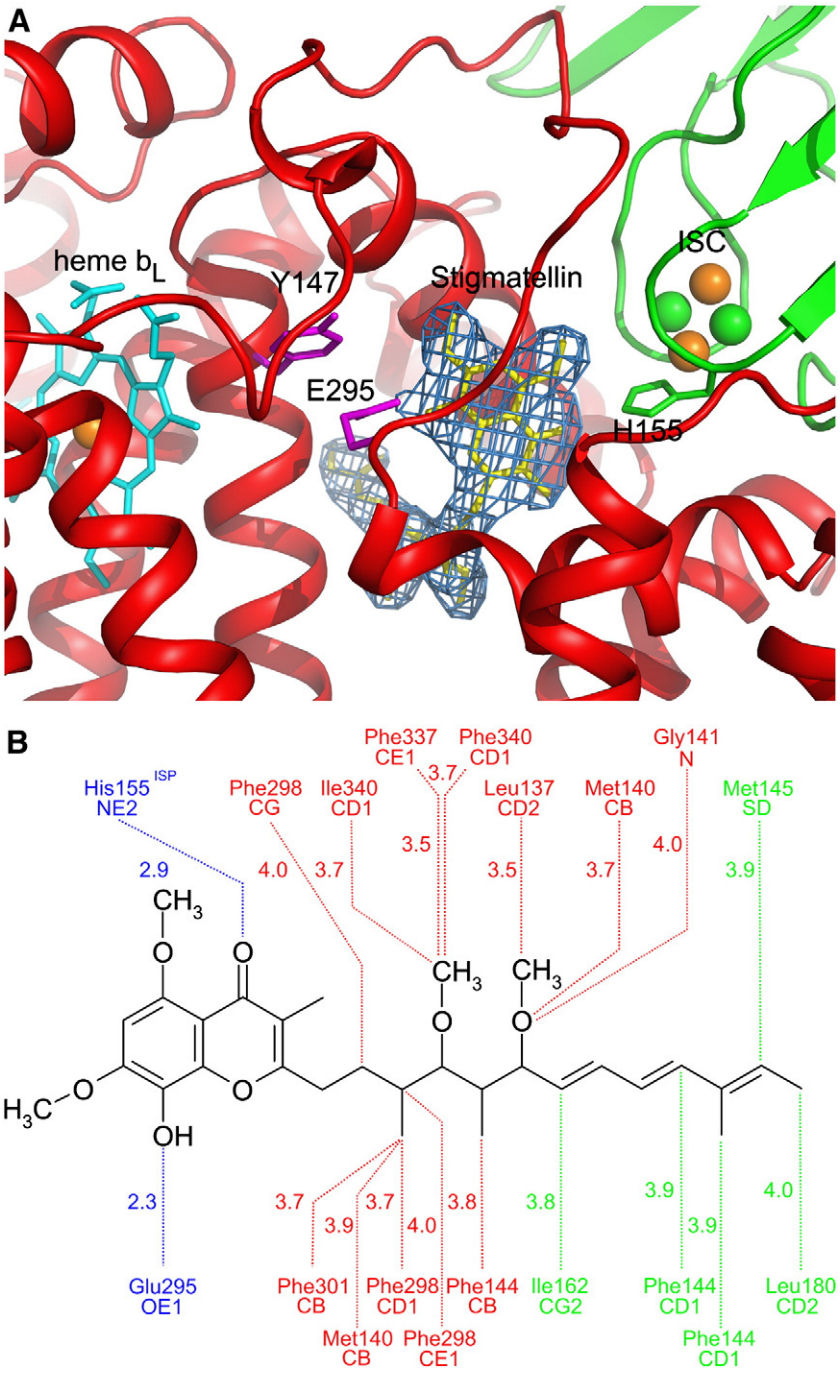

Fig. 5. Binding of the inhibitor stigmatellin to the *P. denitrificans* cyt $bc_1^{\Delta ac}$ complex. A) View into the Q_P site with the bound inhibitor stigmatellin. The F_o–F_c difference electron density map prior to inclusion of the inhibitor is shown as blue mesh representation contoured at 3σ. Stigmatellin, heme b_L and [2Fe–2S] (ISC) are shown in stick or sphere representation. The Cα trace is shown for cyt *b* in red and ISP in green. Side chains of residues $His155^{ISP}$, $E295^{cyt\ b}$ are $Y147^{cyt\ b}$ are depicted as stick model. B) Interactions at the stigmatellin-binding site. H-bonds to the chromone ring are shown in blue, additional interactions with this moiety are omitted for clarity. All interatomic distances of equal to or less than 4 Å are displayed for the proximal and the distal tail in red and green, respectively. For clarity, in cases of multiple interactions fulfilling the distance criterion for the same stigmatellin atom, only the shortest distances are shown.

purified detergent solubilized *P. denitrificans* complex [16], 2.3 nM for the purified reconstituted yeast complex [49] and of 5.7 nM measured in chromatophores of *R. sphaeroides* [2]. In a previous study, Q_P site residues were substituted and the variant complexes analysed for inhibitor sensitivity [16]. Substitution of the direct stigmatellin ligand by glutamine, E295Q, results in 5 fold increase of the IC_{50} value and only 10% residual enzyme activity as compared to the wild type. The only other substitution with a comparably high increase in IC_{50} is $Y147F^{cyt\ b}$, which is not in direct contact with stigmatellin but positioned close (5.8 Å) to the methoxy group of the chromone ring (Fig. 5A) and thus may contribute to binding via an H-bond bridged water molecule [16].

3.7. Cytochrome c_1 and its structurally diverse ISP facing surface

The amino acid sequence numbering used for the description of subunit cyt $c_1^{\Delta ac}$ is based on the variant (Fig. 4). Corresponding residues of wild-type cyt c_1 (Fig. S1) are included in brackets. Cyt $c_1^{\Delta ac}$ consists of a single C-terminal TMH of residues Lys247-Lys281 ($Lys410^{cyt\ c1}$-$Lys444^{cyt\ c1}$) and the N-terminal catalytic domain of residues Ala39-

Pro246 (Ala202$^{cyt\ c1}$-Pro409$^{cyt\ c1}$). The domain houses the cofactor heme c_1 which is bound by the characteristic CXXCH motif with residues Cys82, Cys85, His86 (Cys245$^{cyt\ c1}$, Cys248$^{cyt\ c1}$, His249$^{cyt\ c1}$) and with Met210 (Met373$^{cyt\ c1}$) as the sixth heme ligand. The structure of the subunit is very well defined. In addition to the predicted signal sequence, only few residues are not or poorly resolved at the apparently flexible termini (29 and 6 residues at N- and C-terminus, respectively) and in two loop regions (insertion 1, Ala155-Gly171; loop 4, Glu191-Ala195) and thus omitted from the final structure (Fig. 4C). The overall fold of cyt $c_1^{\Delta ac}$ is similar to mitochondrial and *R. sphaeroides* cyt c_1 as visible for the superimposition of the subunits (Fig. 4). The core of the subunit including the heme cleft is highly conserved (Fig. 4A).

Yet, there are notable differences in four peripheral loop regions (Fig. 4C). Loop 1 close to the membrane surface is slightly shorter in mitochondrial cyt c_1. Loop 2 protrudes from a 2-stranded β-sheet. The longer loop of the yeast complex provides contact with its counterpart from the second monomer at the dimer interface, whereas the loops are about 8 Å apart in *P. denitrificans*. Loop 3 at the rim of the heme cleft holds a short helix in mitochondrial cyt c_1. The *P. denitrificans* loop is similar in position and dimension in contrast to the less extended *R. sphaeroides* loop. The largest heterogeneity is present in the ISP facing loop 4 of *P. denitrificans* (Fig. 4), of which the very tip (5 residues) displays inherent flexibility. The loop is adjacent to insertion 2, a stretch of 18 amino acid residues that are characteristic for *R. sphaeroides* but absent in *P. denitrificans*. In contrast, the 17 amino acid residues long insertion 1 is present in the cyt c_1 primary structure of both *P. denitrificans* and *R. sphaeroides* (Fig. 4C).

One should note that loops 3 and 4 and the insertion 2 contribute to the ISP facing surface. The catalytic ISP domain slides over this surface when alternating between *b* and c_1 position. The very close vicinity of the heme c_1 cleft with its exposed propionate groups is non-polar, except the charge compensating Arg 154 (Arg317$^{cyt\ c1}$) that interacts with one propionate group. Whereas this feature is conserved between *P. denitrificans*, *R. sphaeroides*, and mitochondrial cyt c_1, the rest of the surface varies in respect to contour and charge distribution due to the described differences in loop structures. For instance, the *P. denitrificans* specific loop 4 is close to the ISP domain when the latter is in c_1 position as deduced from superimposition of the *P. denitrificans* domain onto a bovine cyt bc_1 structure in that conformation, whereas the closest loop for the yeast complex in such an orientation would be loop 3 (Fig. 4B). Thus, the ISP facing surface of cyt c_1 is surprisingly diverse between the species even within the family of *Rhodobacteraceae*.

The structural comparison within a bacterial family and with mitochondrial complexes permits an evolutionary interpretation. Noteworthy is the generally higher structural diversity of subunit cyt c_1 as compared to subunits cyt *b* and ISP. The diversity could in principle indicate divergent evolution in reaction to different reaction partners. Whereas cyt *b* and ISP form the evolutionary core of cytochrome *bc* complexes [23], the c-type subunit is more diverse in sequence with different mono- and di-heme cytochromes present in different phyla. The mitochondrial and α-proteobacterial mono-heme cyt c_1 may be evolutionary derived from a collapsed di-heme cytochrome and it seems that the structure of cyt c_1 evolved in the context of the complex and not as soluble mono-heme cyt *c* [24]. Yet, with the structure of *P. denitrificans* cyt bc_1, structural differences of cyt c_1 are now identified even within the family of *Rhodobacteraceae*. That suggests that diversity arises from less structural constraints as compared to other parts of the complex. Specifically, the observed diversity in the ISP-facing cyt c_1 surfaces (Fig. 4B) indicate that a specific cyt c_1:ISP docking interface is not required for electron transfer between the subunits. The ISP in c_1 position brings the [2Fe–2S] cluster closest to heme c_1 as shown with a structure of the bovine cyt bc_1 complex [50]. In that case, the ISP orientation is stabilized by a hydrogen bond between the cluster ligand His161 and one propionate group of heme c_1 as well as by several weak interactions and two additional hydrogen bonds. ISP of *P. denitrificans* can adapt this orientation, as deduced from superimposition to the structure of the bovine complex (Fig. 4B). The hydrogen bond between cluster ligand (His155^{ISP}) and the heme propionate would be kept, whereas the cyt c_1 surface in the vicinity of the cluster-bearing ISP domain differs between mitochondrial, *R. sphaeroides* and *P. denitrificans* complexes. The rate of biological electron transfer is mainly governed by the distance of the redox cofactors with physiological rates at edge-to-edge distances up to 14 Å [44]. The distance between heme c_1 and the [2Fe–2S]-cluster in the superimposed c_1 position is with 10.7 Å well below this limit and would readily permit a fast electron transfer rate which was determined to be $6\times10^4\ s^{-1}$ for *R. sphaeroides* [51]. This electron transfer step is clearly not the rate limiting step for the enzyme activity ($k_{cat} = 120–300\ s^{-1}$). In addition, electron transfer might already occur in intermediate orientations of ISP, when the cluster is approaching the c_1 position. The evolution of diverse structural elements on the ISP facing cyt c_1 surface could either reflect the former or could mean that the hydrogen bond between the essential catalytic moieties of the subunits is central to trap the productive electron transfer complex.

3.8. Model of electron transfer complex with membrane bound cytochrome c

The cyt $bc_1^{\Delta ac}$ complex has an unperturbed cyt c_1 fold and an intact cyt *c* interaction site as shown by superimposition of cyt $c_1^{\Delta ac}$ with yeast cyt c_1 with its bound substrate cyt *c* (Fig. 6). The electron transfer complex was described for yeast cyt bc_1 at high resolution [43]. The acidic domain is most likely laterally associated with the heme-bearing domain of cyt $c_1^{\Delta ac}$ as deduced from the position of the structurally resolved N-terminus at the periphery of the complex (Figs. 2, 6). A similar location is assumed for the flexible acidic N-terminal peptide of 73 residues of yeast QC6p. The structurally resolved N-terminus of the latter has a similar peripheral position (Fig. 6). Interaction with cyt *c* has been suggested as function for both acidic domains [52,53]. Kinetic characterization of the cyt $bc_1^{\Delta ac}$ complex [54] excludes an influence of the acidic domain on catalytic activity, K_M for cyt *c*, and electron transfer rates between cyt c_1 and cyt *c*. The similar structural position supports an analogous function of the acidic domains in *P. denitrificans* and mitochondrial complexes, yet, their role is still elusive.

The structural integrity of cyt $c_1^{\Delta ac}$ is in line with the kinetic characterization of the electron transfer complex, which shows the same k_{cat} and K_M values for variant and wild-type complexes [19,54]. The native substrate of *P. denitrificans* cyt bc_1 is cyt c_{552}, a cyt *c* which is anchored to the membrane by a single N-terminal TMH [55]. Yet, the *P. denitrificans* complex is as promiscuous as other cyt bc_1 complexes and readily reduces cyt *c* from other organisms [16]. Very similar electron transfer rates were also determined between soluble modules of *P. denitrificans* cyt c_1 and its physiological redox partners [56]. This is not surprising as cyt *c* is highly conserved and the interaction between the redox partners seems to employ a conserved interface as shown for the yeast cyt bc_1:cyt *c* complex [1,43,57].

Can the membrane anchored cyt c_{552} dock onto the complex resulting in the same electron transfer complex? The structure of the catalytic soluble domain of cyt c_{552} was described recently at 1.5-Å resolution [58]. A model of the *P. denitrificans* electron transfer complex was built by superimposition of cyt $bc_1^{\Delta ac}$ and cyt c_{552} of the same organism using the high resolution structure of the yeast electron transfer complex as template (Fig. 7). Cyt c_{552} snugly fits in the docking position with exactly superimposed cofactors, a low RMSD of 1.2 Å and without any sterical hindrance neither of the C_α trace nor of the residue side chains. Both electron transfer complexes exhibit highly similar complementary surfaces at the interface. Three of the thirteen modelled interface residue pairs, which coincide with interactions described for the yeast complex, have been previously probed by site directed mutagenesis. In support of the physiological relevance of the model, cyt c_1 variants E243K, A247N and T383C show pronounced reduction of enzyme activity, and E243K and A247N have a reduced intra-molecular electron transfer rate [59].

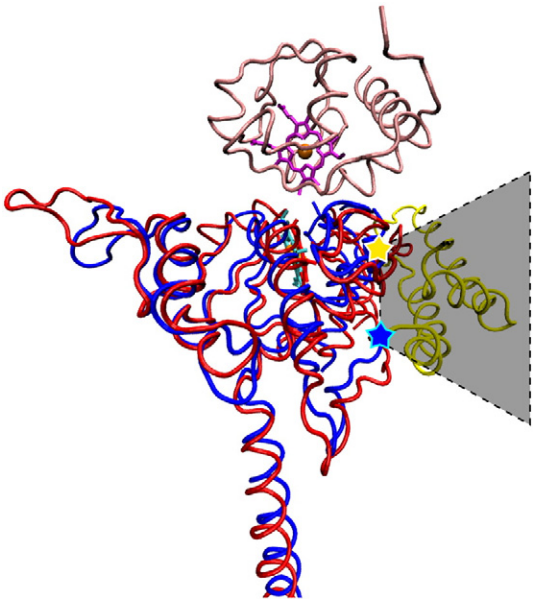

Fig. 6. Superimposition of cyt $c_1^{\Delta ac}$ of *P. denitrificans* (blue) with cyt c_1 from *S. cerevisiae* (red) with bound cyt *c* (pink, PDB 3CX5). Heme c_1 is shown in cyan (*P. denitrificans*) and red (*S. cerevisiae*) and heme *c* in magenta. The yeast electron transfer complex of *S. cerevisiae* is shown together with subunit QCR6p (yellow). The resolved N-termini of QCR6p and cyt $c_1^{\Delta ac}$ are marked with yellow and blue asterisks, respectively. The potential position of the respective acidic domains is indicated by a gray trapezoid. The complex is viewed slightly inclined from an orientation parallel to the membrane plane, with the TMH pointing downwards.

Fig. 7. Modelled ET-complex between the cyt $bc_1^{\Delta ac}$ complex and its native substrate cyt c_{552} of *P. denitrificans*. A) The electron transfer (ET) complex of cyt $bc_1^{\Delta ac}$ complex (cyt $c_1^{\Delta ac}$ blue, cyt *b* red, ISP yellow, hemes cyan) and cyt c_{552} (PDB 3M97, magenta, heme in cyan) was obtained by superimposition with the yeast ET-structure (PDB 3CX5). The position of the membrane anchor (pink) and the linker of cyt c_{552} (dashed line) were modelled according to the given length of the linker and the location of a linker fragment resolved in the cyt c_{552} structure.

Based on the electron transfer model, the position of the transmembrane anchor of cyt c_{552} can be suggested. A flexible linker of 37 amino acid residues, of which a fragment of 12 residues was resolved in the cyt c_{552} structure, connects the catalytic domain with the TMH. Guided by the first resolved residue of a peripheral helix, which is stabilized in position by an H-bond with the catalytic domain, and by the C-terminal half of the linker fragment, the TMH was modelled into a likely docking position at the periphery of the dimeric complex in contact with the transmembrane anchors of cyt c_1 and ISP (Fig. 7). The orientation of the linker fragment may be influenced by a zinc-mediated crystal lattice contact present at the N-terminus of this peptide [58], yet, the given anchor points and the length of the unresolved linker favours this TMH position. In addition, this orientation permits a feasible supercomplex model fulfilling the prerequisite that the catalytic domain of the membrane anchored cyt c_{552} requires access via the same interface to both, the cyt bc_1 complex and cyt *c* oxidase when associated in a respiratory supercomplex shown to exist in *P. denitrificans* [21].

Acknowledgements

This study was supported by the Excellence Initiative of the German Federal and State Governments (EXC 294 to C.H., EXC 115 to B.B., B.L.) and the SFB 472 (German Research Foundation to C.H., B.L.). The authors thank the Diamond Light Source, the European Synchrotron Radiation Facility and the Swiss Light Source for access to beamlines and support by staff during visits. We thank Andrea Herrmann for excellent technical assistance.

Appendix A. Supplementary data

Supplementary data to this article can be found online at doi:10.1016/j.bbabio.2011.09.017.

References

[1] C. Hunte, S. Solmaz, H. Palsdottir, T. Wenz, A structural perspective on mechanism and function of the cytochrome bc (1) complex, Results Probl. Cell Differ. 45 (2008) 253–278.
[2] M.W. Mather, E. Darrouzet, M. Valkova-Valchanova, J.W. Cooley, M.T. McIntosh, F. Daldal, A.B. Vaidya, Uncovering the molecular mode of action of the antimalarial drug atovaquone using a bacterial system, J. Biol. Chem. 280 (2005) 27458–27465.
[3] J.J. Kessl, B.B. Lange, T. Merbitz-Zahradnik, K. Zwicker, P. Hill, B. Meunier, H. Palsdottir, C. Hunte, S. Meshnick, B.L. Trumpower, Molecular basis for atovaquone binding to the cytochrome bc1 complex, J. Biol. Chem. 278 (2003) 31312–31318.
[4] H. Balba, Review of strobilurin fungicide chemicals, J. Environ. Sci. Health B 42 (2007) 441–451.
[5] F.L. Muller, M.S. Lustgarten, Y. Jang, A. Richardson, H. Van Remmen, Trends in oxidative aging theories, Free Radic. Biol. Med. 43 (2007) 477–503.
[6] Z. Zhang, L. Huang, V.M. Shulmeister, Y.I. Chi, K.K. Kim, L.W. Hung, A.R. Crofts, E.A. Berry, S.H. Kim, Electron transfer by domain movement in cytochrome bc1, Nature 392 (1998) 677–684.
[7] D. Xia, C.A. Yu, H. Kim, J.Z. Xia, A.M. Kachurin, L. Zhang, L. Yu, J. Deisenhofer, Crystal structure of the cytochrome bc1 complex from bovine heart mitochondria, Science 277 (1997) 60–66.
[8] E.A. Berry, L.S. Huang, Z. Zhang, S.H. Kim, Structure of the avian mitochondrial cytochrome bc1 complex, J. Bioenerg. Biomembr. 31 (1999) 177–190.
[9] C. Hunte, J. Koepke, C. Lange, T. Rossmanith, H. Michel, Structure at 2.3 Å resolution of the cytochrome bc(1) complex from the yeast *Saccharomyces cerevisiae* co-crystallized with an antibody Fv fragment, Structure 8 (2000) 669–684.
[10] S.R. Solmaz, C. Hunte, Structure of complex III with bound cytochrome c in reduced state and definition of a minimal core interface for electron transfer, J. Biol. Chem. 283 (2008) 17542–17549.
[11] L. Esser, M. Elberry, F. Zhou, C.A. Yu, L. Yu, D. Xia, Inhibitor-complexed structures of the cytochrome bc1 from the photosynthetic bacterium *Rhodobacter sphaeroides*, J. Biol. Chem. 283 (2008) 2846–2857.
[12] E.A. Berry, L.S. Huang, L.K. Saechao, N.G. Pon, M. Valkova-Valchanova, F. Daldal, X-ray structure of *Rhodobacter capsulatus* cytochrome bc (1): comparison with its mitochondrial and chloroplast counterparts, Photosynth. Res. 81 (2004) 251–275.
[13] Y.R. Chen, C.A. Yu, L. Yu, Functional expression of subunit IV of *Rhodobacter sphaeroides* cytochrome b-c1 complex and reconstitution of recombinant protein with three-subunit core complex, J. Biol. Chem. 271 (1996) 2057–2062.
[14] B. Kurowski, B. Ludwig, The genes of the *Paracoccus denitrificans* bc1 complex. Nucleotide sequence and homologies between bacterial and mitochondrial subunits, J. Biol. Chem. 262 (1987) 13805–13811.
[15] R. Covian, T. Kleinschroth, B. Ludwig, B.L. Trumpower, Asymmetric binding of stigmatellin to the dimeric *Paracoccus denitrificans* bc1 complex: evidence for

anti-cooperative ubiquinol oxidation and communication between center P ubiquinol oxidation sites, J. Biol. Chem. 282 (2007) 22289–22297.
[16] T. Kleinschroth, O. Anderka, M. Ritter, A. Stocker, T.A. Link, B. Ludwig, P. Hellwig, Characterization of mutations in crucial residues around the Q(o) binding site of the cytochrome bc(1) complex from *Paracoccus denitrificans*, FEBS J. 275 (2008) 4773–47785.
[17] T. Schroter, O.M. Hatzfeld, S. Gemeinhardt, M. Korn, T. Friedrich, B. Ludwig, T.A. Link, Mutational analysis of residues forming hydrogen bonds in the Rieske [2Fe–2S] cluster of the cytochrome bc1 complex in *Paracoccus denitrificans*, Eur. J. Biochem. 255 (1998) 100–106.
[18] B.L. Trumpower, Cytochrome bc1 complexes of microorganisms, Microbiol. Rev. 54 (1990) 101–129.
[19] M. Castellani, R. Covian, T. Kleinschroth, O. Anderka, B. Ludwig, B.L. Trumpower, Direct demonstration of half-of-the-sites reactivity in the dimeric cytochrome bc(1) complex enzyme with one inactive monomer is fully active but unable to activate the second ubiquinol oxidation site in response to ligand binding at the ubiquinone reduction site, J. Biol. Chem. 285 (2010) 502–510.
[20] R. Covian, B.L. Trumpower, Regulatory interactions in the dimeric cytochrome bc (1) complex: the advantages of being a twin, Biochim. Biophys. Acta 1777 (2008) 1079–1091.
[21] A. Stroh, O. Anderka, K. Pfeiffer, T. Yagi, M. Finel, B. Ludwig, H. Schagger, Assembly of respiratory complexes I, III, and IV into NADH oxidase supercomplex stabilizes complex I in *Paracoccus denitrificans*, J. Biol. Chem. 279 (2004) 5000–5007.
[22] N. Morgner, T. Kleinschroth, H.D. Barth, B. Ludwig, B. Brutschy, A novel approach to analyze membrane proteins by laser mass spectrometry: from protein subunits to the integral complex, J. Am. Soc. Mass Spectrom. 18 (2007) 1429–1438.
[23] M. Schutz, M. Brugna, E. Lebrun, F. Baymann, R. Huber, K.O. Stetter, G. Hauska, R. Toci, D. Lemesle-Meunier, P. Tron, C. Schmidt, W. Nitschke, Early evolution of cytochrome bc complexes, J. Mol. Biol. 300 (2000) 663–675.
[24] F. Baymann, E. Lebrun, W. Nitschke, Mitochondrial cytochrome c1 is a collapsed di-heme cytochrome, Proc. Natl. Acad. Sci. U. S. A. 101 (2004) 17737–17740.
[25] M. Castellani, T. Kleinschroth, R. Covian, B. Ludwig, B.L. Trumpower, Heterodimeric bc(1) complex from *Paracoccus denitrificans*: a validation of the half-of-the-sites mechanism, Bba-Bioenergetics 1797 (2010) 112–113.
[26] V. Zickermann, K. Zwicker, M.A. Tocilescu, S. Kerscher, U. Brandt, Characterization of a subcomplex of mitochondrial NADH:ubiquinone oxidoreductase (complex I) lacking the flavoprotein part of the N-module, Biochim. Biophys. Acta 1767 (2007) 393–400.
[27] M. Fritz, A.L. Klyszejko, N. Morgner, J. Vonck, B. Brutschy, D.J. Muller, T. Meier, V. Muller, An intermediate step in the evolution of ATPases: a hybrid F(0)–V(0) rotor in a bacterial Na(+) F(1)F(0) ATP synthase, FEBS J. 275 (2008) 1999–2007.
[28] A.G. Leslie, The integration of macromolecular diffraction data, Acta Crystallogr. D Biol. Crystallogr. 62 (2006) 48–57.
[29] P. Evans, Scaling and assessment of data quality, Acta Crystallogr. D Biol. Crystallogr. 62 (2006) 72–82.
[30] The CCP4 suite: programs for protein crystallography, Acta Crystallogr. D Biol. Crystallogr. 50 (1994) 760–763.
[31] A.T. Brunger, Free R value: cross-validation in crystallography, Methods Enzymol. 277 (1997) 366–396.
[32] A.J. McCoy, R.W. Grosse-Kunstleve, P.D. Adams, M.D. Winn, L.C. Storoni, R.J. Read, Phaser crystallographic software, J. Appl. Crystallogr. 40 (2007) 658–674.
[33] G.N. Murshudov, A.A. Vagin, E.J. Dodson, Refinement of macromolecular structures by the maximum-likelihood method, Acta Crystallogr. D Biol. Crystallogr. 53 (1997) 240–255.
[34] P. Emsley, K. Cowtan, Coot: model-building tools for molecular graphics, Acta Crystallogr. D Biol. Crystallogr. 60 (2004) 2126–2132.
[35] A.W. Schuttelkopf, D.M. van Aalten, PRODRG: a tool for high-throughput crystallography of protein–ligand complexes, Acta Crystallogr. D Biol. Crystallogr. 60 (2004) 1355–1363.
[36] I.W. Davis, A. Leaver-Fay, V.B. Chen, J.N. Block, G.J. Kapral, X. Wang, L.W. Murray, W.B. Arendall III, J. Snoeyink, J.S. Richardson, D.C. Richardson, MolProbity: all-atom contacts and structure validation for proteins and nucleic acids, Nucleic Acids Res. 35 (2007) W375–383.
[37] W. Humphrey, A. Dalke, K. Schulten, VMD: visual molecular dynamics, J. Mol. Graph. 14 (1996) 33–38.
[38] D. Frishman, P. Argos, Knowledge-based protein secondary structure assignment, Proteins 23 (1995) 566–579.
[39] E.A. Berry, M. Guergova-Kuras, L.S. Huang, A.R. Crofts, Structure and function of cytochrome bc complexes, Annu. Rev. Biochem. 69 (2000) 1005–1075.
[40] K. Pfeiffer, V. Gohil, R.A. Stuart, C. Hunte, U. Brandt, M.L. Greenberg, H. Schagger, Cardiolipin stabilizes respiratory chain supercomplexes, J. Biol. Chem. 278 (2003) 52873–52880.
[41] H. Michel, Characterization and crystal packing of three-dimensional bacteriorhodopsin crystals, EMBO J. 1 (1982) 1267–1271.
[42] M. Caffrey, V. Cherezov, Crystallizing membrane proteins using lipidic mesophases, Nat. Protoc. 4 (2009) 706–731.
[43] S. Solmaz, C. Hunte, Structure of complex III with bound cytochrome c in reduced state and definition of a minimal core interface for electron transfer, J. Biol. Chem. 283 (2008) 17542–17549.
[44] C.C. Page, C.C. Moser, X. Chen, P.L. Dutton, Natural engineering principles of electron tunnelling in biological oxidation–reduction, Nature 402 (1999) 47–52.
[45] C.C. Moser, J.L. Anderson, P.L. Dutton, Guidelines for tunneling in enzymes, Biochim. Biophys. Acta 1797 (2010) 1573–1586.
[46] J.H. Nett, C. Hunte, B.L. Trumpower, Changes to the length of the flexible linker region of the Rieske protein impair the interaction of ubiquinol with the cytochrome bc1 complex, Eur. J. Biochem. 267 (2000) 5777–5782.
[47] H. Tian, S. White, L. Yu, C.A. Yu, Evidence for the head domain movement of the Rieske iron–sulfur protein in electron transfer reaction of the cytochrome bc1 complex, J. Biol. Chem. 274 (1999) 7146–7152.
[48] C.R. Lancaster, C. Hunte, J. Kelley III, B.L. Trumpower, R. Ditchfield, A comparison of stigmatellin conformations, free and bound to the photosynthetic reaction center and the cytochrome bc1 complex, J. Mol. Biol. 368 (2007) 197–208.
[49] T. Wenz, R. Covian, P. Hellwig, F. Macmillan, B. Meunier, B.L. Trumpower, C. Hunte, Mutational analysis of cytochrome b at the ubiquinol oxidation site of yeast complex III, J. Biol. Chem. 282 (2007) 3977–3988.
[50] S. Iwata, J.W. Lee, K. Okada, J.K. Lee, M. Iwata, B. Rasmussen, T.A. Link, S. Ramaswamy, B.K. Jap, Complete structure of the 11-subunit bovine mitochondrial cytochrome bc1 complex, Science 281 (1998) 64–71.
[51] S. Rajagukguk, S. Yang, C.A. Yu, L. Yu, B. Durham, F. Millett, Effect of mutations in the cytochrome b ef loop on the electron-transfer reactions of the Rieske iron–sulfur protein in the cytochrome bc1 complex, Biochemistry 46 (2007) 1791–1798.
[52] M.E. Schmitt, B.L. Trumpower, Subunit 6 regulates half-of-the-sites reactivity of the dimeric cytochrome bc1 complex in *Saccharomyces cerevisiae*, J. Biol. Chem. 265 (1990) 17005–17011.
[53] M. Nakai, T. Endo, T. Hase, Y. Tanaka, B.L. Trumpower, H. Ishiwatari, A. Asada, M. Bogaki, H. Matsubara, Acidic regions of cytochrome c1 are essential for ubiquinol-cytochrome c reductase activity in yeast cells lacking the acidic QCR6 protein, J. Biochem. 114 (1993) 919–925.
[54] M. Castellani, J. Havens, T. Kleinschroth, F. Millett, B. Durham, F. Malatesta, B. Ludwig, The acidic domain of cytochrome c(1) in *Paracoccus denitrificans*, analogous to the acidic subunits in eukaryotic bc(1) complexes, is not involved in the electron transfer reaction to its native substrate cytochrome c(552), Biochim. Biophys. Acta 1807 (2011) 1383–1389.
[55] A. Turba, M. Jetzek, B. Ludwig, Purification of *Paracoccus denitrificans* cytochrome c552 and sequence analysis of the gene, Eur. J. Biochem. 231 (1995) 259–265.
[56] J. Janzon, A.C. Eichhorn, B. Ludwig, F. Malatesta, Electron transfer kinetics between soluble modules of *Paracoccus denitrificans* cytochrome c1 and its physiological redox partners, Biochim. Biophys. Acta 1777 (2008) 250–259.
[57] C. Lange, C. Hunte, Crystal structure of the yeast cytochrome bc1 complex with its bound substrate cytochrome c, Proc. Natl. Acad. Sci. U. S. A. 99 (2002) 2800–2805.
[58] C. Rajendran, U. Ermler, B. Ludwig, H. Michel, Structure at 1.5 Å resolution of cytochrome c(552) with its flexible linker segment, a membrane-anchored protein from *Paracoccus denitrificans*, Acta Crystallogr. D Biol. Crystallogr. 66 (2010) 850–854.
[59] J. Janzon, Q. Yuan, F. Malatesta, P. Hellwig, B. Ludwig, B. Durham, F. Millett, Probing the *Paracoccus denitrificans* cytochrome c(1)-cytochrome c(552) interaction by mutagenesis and fast kinetics, Biochemistry 47 (2008) 12974–12984.
[60] R.A. Engh, R. Huber, Accurate bond and angle parameters for X-ray protein structure refinement, Acta Crystallogr A 47 (1991) 392–400.